THE COLUMN DENSITY VARIANCE IN TURBULENT INTERSTELLAR MEDIA: A FRACTAL MODEL APPROACH

KWANG-IL SEON[1,2]

Draft version November 14, 2012

Abstract

Fractional Brownian motion (fBm) structures are used to investigate the dependency of column density variance ($\sigma_{\ln N}^2$) in the turbulent interstellar medium on the variance of three-dimensional density ($\sigma_{\ln \rho}^2$) and the power-law slope of the density power spectrum. We provide quantitative expressions to infer the three-dimensional density variance, which is not directly observable, from the observable column density variance and spectral slope. We also investigate the relationship between the column density variance and sonic Mach number (M_s) in the hydrodynamic (HD) regime by assuming the spectral slope and density variance as functions of sonic Mach number, as obtained from the HD turbulence simulations. They are related by the expression $\sigma_{\ln N}^2 = A\sigma_{\ln \rho}^2 = A\ln(1+b^2M_s^2)$, suggested by Burkhart & Lazarian for the magneto-hydrodynamic (MHD) case. The proportional constant A varies from ≈ 0.2 to ≈ 0.4 in the HD regime as the turbulence forcing parameter b increases from 1/3 (purely solenoidal forcing) to 1 (purely compressive forcing). It is also discussed that the parameter A is lowered in the presence of a magnetic field.

Subject headings: ISM: structure — ISM: clouds — turbulence

1. INTRODUCTION

A variety of observations and simulations have shown that the density structures of the interstellar medium (ISM) are scale-free, hierarchical, and fractal (e.g., Stutzki et al. 1998; Elmegreen & Scalo 2004; Burkhart et al. 2012). The supersonic, compressible turbulence is likely responsible for the complex and hierarchical density structures observed in the ISM. The density fluctuation due to the supersonic turbulence plays a crucial role in models of star formation rates and initial mass functions (Mac Low & Klessen 2004; Krumholz & McKee 2005; Hennebelle & Chabrier 2008; Federrath & Klessen 2012). Hence, the statistical properties of density structures in the turbulent ISM have been extensively studied in hydrodynamic (HD) and magneto-hydrodynamic (MHD) simulations.

It is now well known that the probability distribution functions (PDFs) of the three-dimensional (3D) densities and column densities of the turbulent ISM are close to lognormal (Vázquez-Semadeni 1994; Nordlund & Padoan 1999; Klessen 2000; Ostriker et al. 2001; Wada & Norman 2001; Burkhart & Lazarian 2012). The standard deviation of density (σ_{ρ/ρ_0}) increases with sonic Mach number, M_s (Nordlund & Padoan 1999; Ostriker et al. 2001). This trend is expressed by $\sigma_{\rho/\rho_0} = bM_s$, where ρ/ρ_0 is the density (ρ) normalized by the mean density (ρ_0) and b is a constant of proportionality, known as the turbulence forcing parameter. Values of b ranging from ≈ 0.3 to ≈ 1.0 have been suggested in numerical simulations (Padoan et al. 1997; Passot & Vázquez-Semadeni 1998; Kritsuk et al. 2007; Beetz et al. 2008). Federrath et al. (2008, 2009, 2010) have found that for the same M_s, compressive (dilatational) forcing leads to much larger density variance compared to solenoidal (rotational) forcing. They showed that b depends on the type of the turbulence forcing varying from $\approx 1/3$ for solenoidal forcing to ≈ 1 for compressive forcing.

The density power spectrum is also a useful tool to characterize the turbulent ISM. The power spectra of turbulent clouds are power laws in form (Crovisier & Dickey 1983; Despande et al. 2000; Stanimirović & Lazarian 2001; Padoan et al. 2004). Kim & Ryu (2005) have investigated the dependency of the power-law slope of the density power spectrum on M_s and found that the density spectrum becomes gradually shallower as M_s increases in HD turbulent media. Kowal et al. (2007) and Burkhart et al. (2010) confirmed the flattening of the density spectra with M_s in MHD cases. Federrath et al. (2009) showed that compressive forcing leads to significantly steeper density spectra than solenoidal forcing.

We note that the spectral slope of the 3D density power spectrum is the same as that of the projected column density power spectrum (e.g., Stutzki et al. 1998; Padoan et al. 2004) and thus can be directly extracted from observations. On the other hand, the 3D density is not an observationally accessible quantity, but instead the column density, i.e., the integral of the density along a line of sight, is observable. There is a great deal of observational data, which traces the ISM column density, from surveys. Some examples are the GALFA (Peek et al. 2011) and GASKAP (Dickey et al. 2012) H I surveys and Columbia-Cfa (Dame et al. 2001) and ThrUMMS[3] molecular gas surveys. The best way to infer the variance of the 3D density field from observations is obviously to compare the observational data with a large number of turbulence simulations. However, instead of performing expensive simulations, a simpler approach to derive the 3D density variance would be of great interest. Padoan et al. (1997) generated random density distributions with various density variances and spectral slopes and compared the resulting synthesized extinction maps with the observed extinction data. Brunt et al. (2010) developed an interesting technique for calculating the variance of a 3D density field using only information contained in the two dimensional projection. The technique has been applied to the Taurus molecular cloud (Brunt 2010). More recently, Burkhart & Lazarian (2012) found a column

[1] Korea Astronomy and Space Science Institute, Daejeon 305-348, Republic of Korea; kiseon@kasi.re.kr
[2] University of Science and Technology, Daejeon 305-350, Republic of Korea
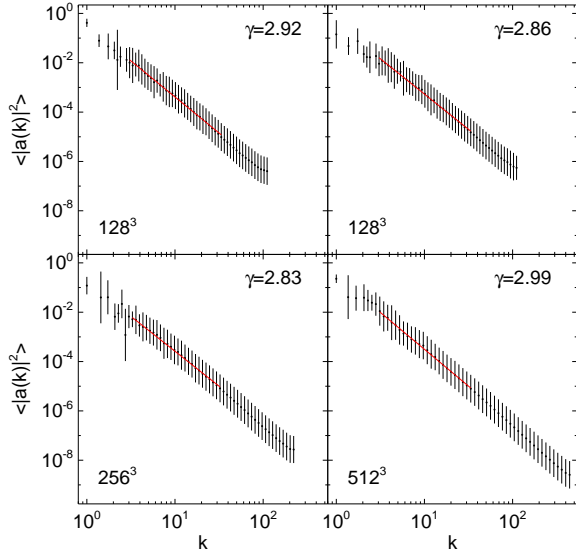
[3] http://www.astro.ufl.edu/~peterb/research/thrumms/

Figure 1. Examples density power spectra with the 128^3, 256^3, and 512^3 resolutions, which were obtained for $(\gamma_g, \sigma_{\ln \rho}) = (3.4, 1.4)$. Error bars denote standard deviations in wavenumber bins. The best-fit lines and slopes, which were obtained over the range $3 \leq k \leq 35$, are also shown.

Figure 2. Spectral slopes (γ) of lognormal density fields vs. the original spectral slopes (γ_g) of the Gaussian density fields. Best-fit polynomial curves for every density variance $\sigma_{\ln \rho}$ are also shown. The circles and curves were shifted vertically by the amounts of Δ for clarity.

density variance-Mach number relationship, using MHD simulations. The relationship closely follows the form of the 3D density variance-Mach number relationship but includes a scaling parameter A such that

$$\sigma_{\ln N}^2 = A \ln(1 + b^2 M_s^2), \tag{1}$$

where $\sigma_{\ln N}^2$ is the variance of the logarithm of the column density N[4].

In the present study, quantitative expressions relating the 3D density variance, spectral slope, and column density variance are obtained by using the fractional Brownian motion (fBm) algorithm (Saupe 1988; Stutzki et al. 1998; Elmegreen 2002). A lognormal density field is obtained by generating a Gaussian random field with a power-law spectral slope (γ_g) and exponentiating the field (Elmegreen 2002). This letter is organized as follows. In Section 2, we describe how to infer the variance of the 3D density field from the given spectral slope and column density variance. Section 3 investigates the $\sigma_{\ln N}^2 - M_s$ relationship. Concluding remarks are given in Section 4.

2. MODEL OF THE LOGNORMAL DENSITY FIELD

The fBm structures are generated by first assigning 3D Fourier coefficients following the prescription of Elmegreen (2002). The Fourier amplitudes are generated to be distributed as a normal Gaussian with the variance $< |a(\mathbf{k})|^2 > = |\mathbf{k}|^{-\gamma_g}$. The inverse Fourier transform gives a Gaussian random field $\rho_g(\mathbf{x})$. We then multiply the density field with the desired standard deviation of the logarithmic density $\sigma_{\ln \rho}$, and exponentiate the field to obtain $\rho = \exp(\sigma_{\ln \rho} \rho_g)$.

The standard deviation $\sigma_{\ln N}$ depends on both γ_g and $\sigma_{\ln \rho}$. We should also note that the spectral slopes γ of resulting lognormal density fields are different from the input slopes γ_g. Therefore, we need to find the relationship between the input variables (γ_g, $\sigma_{\ln \rho}$) and the outputs (γ, $\sigma_{\ln N}$). In addition, the generated density fields with the same parameters (γ_g, $\sigma_{\ln \rho}$)

---

[4] Note that $\sigma_{\ln N/N_0} = \sigma_{\ln N}$, but $\sigma_{N/N_0} = \sigma_N/N_0$ for the mean column density N_0. The same relationships are applied to the 3D density ρ.
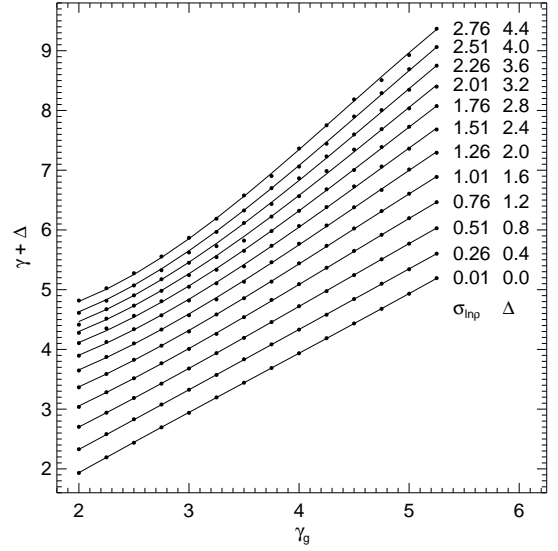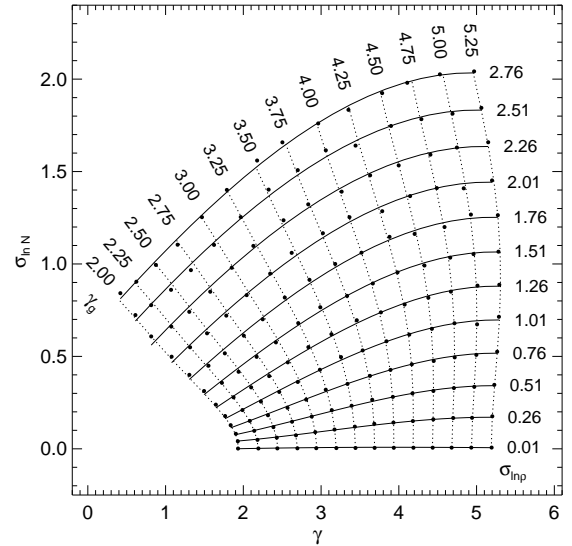

Figure 3. The column density deviations $\sigma_{\ln N}$ and spectral slopes γ of lognormal density fields obtained for various combinations of $\sigma_{\ln \rho}$ and γ_g of the Gaussian random field. Solid and dotted lines are best-fit curves tracing the ($\sigma_{\ln N}, \gamma$) pairs corresponding to constant $\sigma_{\ln \rho}$ and γ_g, respectively.

show large fluctuations due to random phases and amplitudes in Fourier space. We thus generated a large volume of lognormal density fields by varying γ_g and $\sigma_{\ln \rho}$ and obtained the average relationships between the parameters. We varied γ_g from 2.0 to 5.25 in steps of 0.25 and $\sigma_{\ln \rho}$ from 0.01 to 2.76 in steps of 0.25. One hundred random realizations with a box size of 128^3 were generated for each combination of γ_g and $\sigma_{\ln \rho}$, resulting in a total of 16,800 realizations. We also generated 30 realizations with a resolution of 256^3 for every (γ_g, $\sigma_{\ln \rho}$) pair and confirmed that the 256^3 dataset is consistent with the results obtained with the 128^3 resolution. As will be shown later, the present results are also consistent with the limited samples obtained with a box size of 512^3. The standard deviations and spectral slopes were calculated for

Table 1
Polynomial coefficients for γ as a function of $(\gamma_g, \sigma_{\ln\rho})$, and for γ_g and $\sigma_{\ln\Sigma}$ as functions of $(\gamma, \sigma_{\ln\rho})$.

	p_0	p_1	p_2	p_3	p_4
a_0	$-2.582(-1)$	$6.609(-1)$	1.242	-1.040	$2.019(-1)$
a_1	1.185	$-6.876(-1)$	-1.019	$7.400(-1)$	$-1.462(-1)$
a_2	$-5.344(-2)$	$2.080(-1)$	$2.316(-1)$	$-1.827(-1)$	$3.865(-2)$
a_3	$4.832(-3)$	$-1.928(-2)$	$-1.395(-2)$	$1.395(-2)$	$-3.283(-3)$
b_0	$2.841(-1)$	$-9.168(-1)$	$-9.334(-1)$	1.221	$-2.546(-1)$
b_1	$8.173(-1)$	$5.994(-1)$	1.326	-1.125	$2.119(-1)$
b_2	$5.019(-2)$	$-1.468(-1)$	$-3.838(-1)$	$2.970(-1)$	$-5.417(-2)$
b_3	$-4.428(-3)$	$1.186(-2)$	$3.111(-2)$	$-2.375(-2)$	$4.329(-3)$
c_0	$-2.336(-2)$	$6.929(-1)$	-1.516	$8.404(-1)$	$-1.278(-1)$
c_1	$1.826(-2)$	$-6.199(-1)$	1.099	$-4.586(-1)$	$5.987(-2)$
c_2	$-4.381(-3)$	$2.381(-1)$	$-2.647(-1)$	$9.389(-2)$	$-1.117(-2)$
c_3	$3.689(-4)$	$-2.369(-2)$	$2.235(-2)$	$-7.710(-3)$	$9.542(-4)$

Note: The numbers in parentheses are exponents on 10, meaning that $6.609(-1) = 6.609 \times 10^{-1}$.

every realization and averaged to obtain the ensemble average values of $(\gamma, \sigma_{\ln N})$ for each combination of the input $(\gamma_g, \sigma_{\ln\rho})$ values. The power spectra of resulting lognormal density fields show a slight flattening at large wavenumbers. Examples of the spectra are shown in Figure 1. Spectral slopes were obtained by least-squares fits over a wavenumber range of $3 \le k \le 35$. Here, the dimensionless wavenumber is defined by $k = L/\lambda$ with the wavelength λ and box size L.

For ease of use, we parameterized the relationships between the parameters γ, γ_g, $\sigma_{\ln\rho}$, and $\sigma_{\ln N}$ using polynomials. For every $\sigma_{\ln\rho}$, $\sigma_{\ln N}$ was parameterized with a cubic function of γ, i.e.,

$$\sigma_{\ln N} = \sum_{i=0}^{3} c_i \gamma^i = c_0 + c_1\gamma + c_2\gamma^2 + c_3\gamma^3. \quad (2)$$

The coefficients c_i ($i = 0, \dots, 3$) were then fitted with a quartic polynomial of $\sigma_{\ln\rho}$, i.e.,

$$c_0 = \sum_{j=0}^{4} p_j \sigma_{\ln\rho}^j = p_0 + p_1\sigma_{\ln\rho} + p_2\sigma_{\ln\rho}^2 + p_3\sigma_{\ln\rho}^3 + p_4\sigma_{\ln\rho}^4. \quad (3)$$

In this way, $\sigma_{\ln N}$ could be estimated as a function of γ_g and $\sigma_{\ln\rho}$. We also parameterized γ with a cubic function of γ_g and γ_g with another cubic function of γ for every $\sigma_{\ln\rho}$, i.e., $\gamma = \Sigma_i a_i \gamma_g^i$ and $\gamma_g = \Sigma_i b_i \gamma^i$ ($i = 0, \dots, 3$). The coefficients a_i and b_i ($i = 0, \dots, 3$) were then fitted with quartic polynomial functions of $\sigma_{\ln\rho}$, as done for the coefficients c_i.

The final coefficients are shown in Table 1. Figure 2 shows the resulting γ's as functions of γ_g for every $\sigma_{\ln\rho}$. Figure 3 presents the resulting $(\gamma, \sigma_{\ln N})$ pairs for every $(\gamma_g, \sigma_{\ln\rho})$ pair. In the figures, the solid and dotted lines are the best-fit polynomials to reproduce the $(\gamma, \sigma_{\ln N})$ pairs corresponding to constant $\sigma_{\ln\rho}$ and γ_g, respectively.

The power spectra of lognormal density (ρ) fields are usually shallower than those of the original Gaussian density ($\ln\rho$) fields, i.e., $\gamma < \gamma_g$. The property that the power spectra of $\ln\rho$ are stiffer than those of ρ in turbulence simulations is also noticeable in Table 2 of Kowal et al. (2007). The difference between γ and γ_g becomes more significant for a larger $\sigma_{\ln\rho}$ and for shallower (smaller) γ_g. Column density variance is always smaller than the variance of 3D density, as expected. The ratio of $\sigma_{\ln N}$ to $\sigma_{\ln\rho}$ becomes smaller for a shallower γ. This is caused by less spatial correlation in the
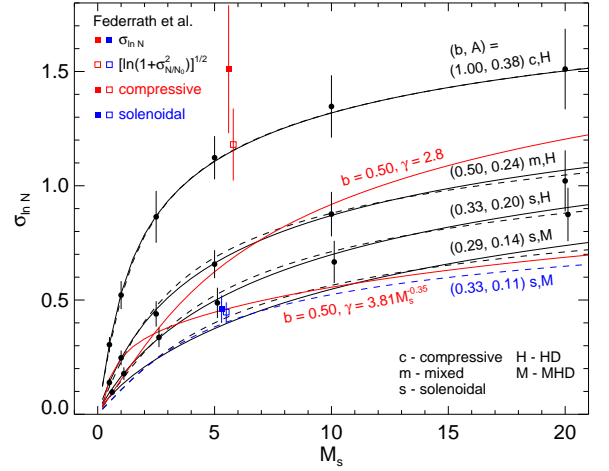

Figure 4. Column density variance-Mach number relationship. The upper three black-curves represent the cases of compressive ($b = 1$), mixing ($b = 0.5$), and solenoidal mode ($b = 1/3$). The lowest black curves are obtained by assuming $b = 0.29$ and $\gamma = 3.81M_s^{0.16} - 0.3$ to mimic the magnetic field effects. Dashed black lines represent the best-fit results to Equation (1) with the parameters (b, A) denoted along the curves. Dashed blue line shows the curve of Burkhart & Lazarian (2012). Forcing types (c, m, s) and the simulation regimes (H, M) are also denoted. Red lines are obtained by varying the $\gamma - M_s$ relationship arbitrarily and demonstrate that Equation (1) is not satisfied unless proper relationships between γ and M_s are assumed.

density fields with a shallower spectral slope. For instance, the density fields with $\gamma = 0$ have no spatial correlation.

The equations relating γ and γ_g will be useful in generating the realistic ISM density structures. The equation relating $\sigma_{\ln N}$ to γ and $\sigma_{\ln\rho}$ or Figure 3 provides a tool to derive $\sigma_{\ln\rho}$ from the observable $\sigma_{\ln N}$ and γ. Once we obtain γ and $\sigma_{\ln N}$ from observations, we can vary $\sigma_{\ln\rho}$ to find the best-fit value that gives the observed $\sigma_{\ln N}$.

3. COLUMN DENSITY VARIANCE-MACH NUMBER RELATIONSHIP

We now investigate the relationship between $\sigma_{\ln N}$ and M_s by using the expressions derived in Section 2. In the above, we have assumed that γ and $\sigma_{\ln\rho}$ are independent variables. However, γ and $\sigma_{\ln\rho}$ are not independent in the real turbulent media, but rather depend on M_s. If we ignore magnetic fields, the statistical properties are uniquely determined by M_s and b. We therefore need to specify the dependencies of γ and $\sigma_{\ln\rho}$ on M_s.

Seon (2009) combined the results of Kim & Ryu (2005), Kritsuk et al. (2006), and Padoan et al. (2004), and obtained a simple relation between M_s and γ, i.e., $\gamma = 3.81M_s^{-0.16}$, which may be applicable to solenoidal forcing. The power spectra of the compressively driven turbulence are considerably steeper than those of the solenoidal forcing. The spectral slopes at $M_s \approx 2.3$ and 5.6 for compressive forcing are provided by Schmidt et al. (2009) and Federrath et al. (2009), respectively, and are ~ 0.6 larger than the values for the solenoidal case. We therefore assume that $\gamma = 3.81M_s^{-0.16} + 0.6$ for the compressive mode. There are two transverse (solenoidal) and one longitudinal (compressive) wave mode in the 3D space. Therefore, the solenoidal and compressive forcing would be mixed with a ratio of 2:1 if no preferential forcing mode were provided (Federrath et al. 2010). The power spectrum of this natural mixing mode might be obtained by adding two power spectra for solenoidal and compressive forcing with a ratio of 2:1. The resulting power spectrum is also represented by a power-law with a spectral slope, which is at most ~ 0.06 larger than the slope of the solenoidal case. We therefore as-

sume the same spectral slope as the solenoidal forcing case for the natural mixing case.

The density variance in logarithmic scale is obtained from the variance in linear scale using the property of a lognormal distribution, i.e., $\sigma_{\ln\rho}^2 = \ln(1+\sigma_{\rho/\rho_0}^2) = \ln(1+b^2 M_s^2)$. The forcing parameter b is $1/3$, 0.5, and 1 for solenoidal, natural mixing, and compressive modes, respectively (Federrath et al. 2008, 2009, 2010).

Using γ and $\sigma_{\ln\rho}$ as functions of M_s, and Equation (2), we calculate $\sigma_{\ln N}$ for solenoidal, natural mixing, and compressive modes as functions of M_s. The results are shown in Figure 4, wherein the upper three black-curves show $\sigma_{\ln N}$ as functions of M_s for three different forcing types. We fitted the obtained curves with Equation (1). The best-fit A values are found to be 0.2, 0.24, and 0.38 for the solenoidal, natural mixing, and compressive modes, respectively. In Figure 4, the b and best-fit A values are denoted in parentheses along the curves. The best-fit curves are shown as dashed lines.

Applying the expression relating γ and γ_g derived with the 128^3 dataset, we also generated the lognormal density fields with a higher resolution of 512^3 for $M_s = 0.5$, 1, 2.5, 5, 10, and 20. For every combination of parameters (b, M_s), we produced 30 realizations and calculated the ensemble average of $\sigma_{\ln N}$ and its statistical dispersion. Circles and error bars in Figure 4 represent the ensemble averages and the dispersions, respectively, which closely follow the curves calculated with the 128^3 dataset. We therefore conclude that the expressions obtained with a rather lower resolution of 128^3 are also applicable to the higher resolution of 512^3. The error bars obtained with the 512^3 resolution indicate the ranges of variation between realizations.

In Figure 4, we over-plotted the data points obtained from the HD simulations with solenoidal (blue squares) and compressive forcing (red squares) modes of Federrath et al. (2010), who provide the standard deviations of linear column density (σ_{N/N_0}) and logarithmic column density ($\sigma_{\ln N}$). The filled squares show the $\sigma_{\ln N}$ values that they directly measured with the logarithmic column density and the open squares represent the values $[\ln(1+\sigma_{N/N_0}^2)]^{1/2}$ calculated with the standard deviations of the column density σ_{N/N_0} assuming that the column density PDF is a perfect lognormal distribution. The values estimated with the two different methods show a significant discrepancy, especially for compressive mode, indicating that the column density PDF is not a perfect lognormal (see also Price et al. 2011 for the discrepancies). Indeed, the PDFs for compressive forcing show large departures from a perfect lognormal function (Federrath et al. 2010). Even with this departure from the perfect lognormal function, the present results are consistent with their results within the variation ranges denoted by error bars in the figure.

In the above analyses, we have assumed HD cases. Burkhart & Lazarian (2012) fitted the MHD simulation results for solenoidal forcing with Equation (1) and obtained a best-fit A of 0.11, which is different from our result of $A = 0.2$. The difference might be attributable to the magnetic field effects. First, the density variance in magnetized gas is significantly lower than that in the HD counterparts (Ostriker et al. 2001; Price et al. 2011; Molina et al. 2012). The effect could be mimicked by reducing b below the value of the HD case, while assuming the same relationship between γ and M_s for the HD case. We found that the $\sigma_{\ln N}^2 - M_s$ relationship derived with $b = 0.22$ is very close to the result of

Burkhart & Lazarian (2012). Second, the spectral slope of the strongly magnetized media appears to be shallower than those of unmagnetized or weakly magnetized media. Padoan et al. (2004) found that the MHD model with approximate equipartition of kinetic and magnetic energies yields a shallower density power spectrum than the super-Alfvénic model. The results of Kowal et al. (2007) also provide some indications that the power-law slopes of the supersonic, sub-Alfvénic models are slightly smaller than those of super-Alfvénic models. Their spectral slopes for the cases of a strong magnetic field are lower than the values expected from $\gamma = 3.81 M_s^{-0.16}$ by amounts of $\sim 0.3-0.4$. Indeed, we could reproduce the best-fit curve of Burkhart & Lazarian (2012) with a spectral slope of $\gamma = 3.81 M_s^{-0.16} - 0.5$ and $b = 1/3$. In a real situation, both effects may play roles together. Therefore, we lowered both γ and b and found that the results with $\gamma = 3.81 M_s^{-0.16} - 0.3$ and $b = 0.29$ match the result of Burkhart & Lazarian (2012), as shown by the lowest black curve in Figure 4. In the figure, the black and blue dashed lines denote the best-fit results to Equation (1) with $b = 0.29$ and $b = 1/3$, respectively.

Burkhart et al. (2010) presented γ as a function of M_s for MHD simulations with different magnetic field strengths and found that the magnetic field effect on γ is more important at lower M_s than at higher M_s. Therefore, we may need further investigations on the magnetic field effects.

Another aspect worth noting is that we can constrain the condition for Equation (1) to hold, by varying the equation between γ and M_s. For instance, in Figure 4, we plotted the $\sigma_{\ln N} - M_s$ relationship by assuming a constant spectral slope of $\gamma = 2.8$ (upper red curve) for $b = 0.5$. It is obvious that the resulting curve cannot be expressed by Equation (1). As we assume γ increases with M_s, we obtain more rapidly increasing curves than the red curve. On the other hand, if we assume γ decreases more rapidly than $\gamma = 3.81 M_s^{-0.16}$ with increasing M_s, the resulting curve shows a much slower increase with increasing M_s, as indicated by the lower red curve obtained for $\gamma \propto M_s^{-0.35}$. Therefore, we conclude that the necessary condition for Equation (1) is that the spectral slope should moderately decrease as M_s increases.

4. CONCLUDING REMARKS

We investigated the dependency of the column density variance on the 3D density variance and the power-law slope of the density power spectrum by using the fBm structures. Adopting the spectral slopes and 3D density variances that are appropriate in the HD regime, we obtained the same relationship between the column density variance and the Mach number as suggested by Burkhart & Lazarian (2012), but with a different scaling parameter A. However, when the magnetic field effects were included, the parameter A agreed with the MHD result of Burkhart & Lazarian (2012). Magnetic fields prevent the turbulent gas from reaching very low densities as well as very high densities (Molina et al. 2012), and consequently have important implications for the models of the star formation rate (e.g., Federrath & Klessen 2012).

The approach adopted in this letter is similar to that of Padoan et al. (1997) in the point that they also use random density fields to derive the 3D density variance. The fBm structures also have been used to investigate the density structure of molecular clouds (Stutzki et al. 1998) and the stellar initial mass function (Elmegreen 2002; Shadmehri & Elmegreen 2012). Note that Stutzki et al. (1998) neglected the dispersion in Fourier amplitudes in gen-

erating Gaussian random fields. We compared the cases of fixed Fourier amplitudes with the results presented here, and found that the fixed amplitudes give rise to slightly stiffer spectral slopes than the present results.

The present results can be applied directly to the observations to infer the 3D density variance from the observed column density variance and spectral slope. We can vary $\sigma_{\ln \rho}$ in Equations (2) and (3) to find the best-fit value that matches the observed $\sigma_{\ln N}$. In applying the results, we need to consider the effects of instrument noise and telescope smoothing. However, the inclusion of noise and smoothing may not severely affect the applicability of the results, as in Burkhart & Lazarian (2012).

The density fluctuation of the ISM plays a crucial role in understanding the propagation of radiation. The intensity PDF of the dust-scattered starlight in far-ultraviolet was found to be lognormal, which might be caused by the density structure of interstellar dust (Seon et al. 2011). Escape of the ionizing radiation field through the clumpy ISM has been argued to be the origin of ubiquitous diffuse ionized gas (e.g., Haffner et al. 2009). This has not, however, been clearly confirmed using realistic ISM density structures (c.f., Seon 2009; Seon & Witt 2012). The present study provides a practical method to generate the realistic density structures for the radiative transfer problems.

REFERENCES

Beetz, C., Schwarz, C., Dreher, J., & Grauer, R. 2008, Phys. Rev. A, 372, 3037
Brunt, C. M. 2010, A&A, 513, A67
Brunt, C. M., Federrath, C., & Price, D. J. 2010, MNRAS, 403, 1507
Burkhart, B., & Lazarian, A. 2012, ApJ, 755, L19
Burkhart, B., Lazarian, A., Goodman, A., & Rosolowsky, E. 2012, submitted to ApJ, arXiv:1206.4703v1
Burkhart, B., Stanimirovic, S., Lazarian, A., & Kowal, G. 2010, ApJ, 708, 1204
Crovisier, J., & Dickey, J. M. 1983, A&A, 122, 282
Dame, T. M., Hartmann, D., & Thaddeus, P. 2001, ApJS, 547, 792

Deshpande, A. A., Dwarakanath, K. S., & W M Goss, 2000, 543, 227
Dickey J. M., McClure-Griffiths, N., Gibson, S. J., et al., 2012, PASA, in press (arXiv:1207.0891)
Elmegreen, B. G. 2002, ApJ, 564, 773
Elmegreen, B. G., & Falgarone, E. 1996, ApJ, 471, 816
Elmegreen, B. G., & Scalo, J. 2004, ARA&A, 42, 211
Federrath, C., Klessen, R. S., & Schmidt, W. 2008, ApJ, 688, L79
Federrath, C., Klessen, R. S., & Schmidt, W. 2009, ApJ, 692, 364
Federrath, C., Roman-Duval, J., Klessen, R. S., Schmidt, W., & Mac Low, M.-M., 2010, A&A, 512, A81
Federrath, C., & Klessen, R. S. 2012, ApJ, accepted (arXiv:1209.2856v2)
Haffner, L. M., Dettmar, R.-J., Beckman, J. E., et al. 2009, Rev. of Mod. Phys., 81, 696
Hennebelle, P., & Chabrier, G. 2008, ApJ, 684, 395
Klessen, R. S. 2000, ApJ, 535, 869
Kim, J., & Ryu, D. 2005, ApJ, 630, L45
Kowal, G., Lazarian, A., & Beresnyak, A. 2007, ApJ, 658, 423
Kritsuk, A. G., Norman, M. L., & Padoan, P. 2006, ApJ, 638, L25
Kritsuk, A. G., Norman, M. L., Padoan, P., & Wagner, R. 2007, ApJ, 665, 416
Krumholz, M. R., & McKee, C. F. 2005, ApJ, 630, 250
Mac Low, M.-M., & Klessen, R. S. 2004, Rev. Mod. Phys., 76, 125
Molina, F. Z., Glover, S. C. O., Federrath, C., & Klessen, R. S. 2012, MNRAS, 423, 2680
Nordlund, A., & Padoan, P. 1999, in Interstellar Turbulence, ed. J. Franco & A. Carramiñana (Cambridge : Cambridge Univ. Press), 218
Ostriker, E. C., Stone, J. M., & Gammie, C. F. 2001, ApJ, 546, 980
Padoan, P., Jones, B. J. T., & Nordlund, Å. 1997, ApJ, 474, 730
Padoan, P., Jimenez, R., Juvela, M., & Nordlund, Å. 2004, ApJ, 604, L49
Passot, T., & Vázquez-Semadeni, E. 1998, Phys. Rev. E, 58, 4501
Peek, J. E. G., Heiles, C., Douglas, K. A., et al. 2011, ApJS, 194, 20
Price, D. J., Federrath, C., Brunt, C. M. 2011, ApJ, 727, L21
Saupe, D. 1988, in The Science of Fractal Images, ed. H. O. Peitgen, & D. Saupe (New York : Springer), 71
Seon, K.-I. 2009, ApJ, 703, 1159
Seon, K.-I., Edelstein, J., Korpela, E. J., et al. 2011, ApJS, 196, 15
Seon, K.-I., & Witt, A. N. 2012, ApJ, 758, 109
Schmidt, W., Federrath, C., Hupp, M., Kern, S., & Niemeyer, J. C. 2009, A&A, 494, 127
Shadmehri, M., & Elmegreen, B. G. 2012, MNRAS, 410, 788
Stanimirović, S., & Lazarian, A. 2001, ApJ, 551, L53
Stutzki, J., Bensch, F., Heithausen, A., Ossenkopf, V., & Zielinsky, M. 1998, A&A, 336, 697
Vázquez-Semadeni, E. 1994, ApJ, 423, 681
Wada, K., & Norman, C. A. 2001, ApJ, 547, 172